Mon. Not. R. Astron. Soc. **356,** 859–871 (2005) doi:10.1111/j.1365-2966.2004.08535.x

Spine–sheath polarization structures in four active galactic nuclei jets

A. B. Pushkarev,[1⋆] D. C. Gabuzda,[2] Yu. N. Vetukhnovskaya[3] and V. E. Yakimov[4]

[1]*Pulkovo Observatory, 196140 St. Petersburg, Russia*
[2]*Physics Department, University College Cork, Cork, Ireland*
[3]*Pushchino Astronomy Observatory, Moscow, Russia*
[4]*Astro Space Centre, Moscow, Russia*

Accepted 2004 October 25. Received 2004 September 26; in original form 2004 June 9

ABSTRACT

We present the results of multifrequency (15 + 8 + 5 GHz) polarization Very Long Baseline Array (VLBA) observations of the three BL Lacertae objects 0745+241, 1418+546 and 1652+398 together with 5-GHz VLBI Space Observatory Programme (VSOP) observations of 1418+546 and 1.6- and 5-GHz VSOP observations of the blazar 1055+018. The jets of all these sources have polarization structure transverse to the jet axis, with the polarization ***E*** vectors aligned with the jet along the jet spine and 'sheaths' of orthogonal ***E*** vectors at one or both edges of the jet. The presence of polarization aligned with the jet near the 'spine' may indicate that the jets are associated with helical ***B*** fields that propogate outward with the jet flow; the presence of orthogonal polarization near the edges of the jet may likewise be a consequence of a helical jet ***B*** field, or may be owing to an interaction with the ambient medium on parsec scales. We have tentatively detected interknot polarization in 1055+018 with ***E*** aligned with the local jet direction, consistent with the possibility that the jet of this source is associated with a helical ***B*** field.

Key words: magnetic fields – polarization – BL Lacertae objects: general.

1 INTRODUCTION

BL Lacertae (BL Lac) objects are active galactic nuclei with weak, sometimes undetectable, optical line emission and strong variability in total intensity and linear polarization over a wide wavelength range from ultraviolet to radio. They usually have point-like optical images and compact radio structure, with flat or inverted radio spectra. The radio emission and much of the optical emission is believed to be synchrotron radiation. With the exception of the weakness of the optical line emission, these properties are shared by optically violently variable (OVV) quasars. Rapidly variable BL Lac objects and OVV quasars are sometimes referred to collectively as 'blazars'.

Previous very long baseline inferometry (VLBI) polarization observations of radio-bright BL Lac objects have showed certain characteristic properties on parsec scales: one-sided core-jet structures having superluminal motions with typical speeds on average lower than those in quasars; polarization ***E***-vector position angles, χ, parallel to the local jet axis, and a tendency for the core χ values to lie either parallel or perpendicular to the jet axis (Gabuzda, Pushkarev & Cawthorne 2000). Jet components are typically optically thin (as is indicated by both their spectral indices and degrees of polarization). Therefore, the tendency for the jet χ vectors to align with the jet direction implies that the associated magnetic field ***B*** is predominantly transverse. This has usually been taken as evidence of relativistic shocks (Laing 1980; Hughes, Aller & Aller 1989), which we observe as distinct jet knots. Alternatively, such transverse fields could reflect the presence of helical ***B*** fields associated with the jets (Gabuzda 1999; Pushkarev & Gabuzda 2000; Gabuzda & Pushkarev 2001). One interesting consequence of this latter scenario is that, depending on the viewing angle, helical jet ***B*** fields can give rise to a 'spine–sheath' polarization structure in the frame of the observer, with a region of longitudinal polarization along the central ridge line of the jet surrounded by regions of orthogonal polarization near the jet edges (Laing 1996; Lyutikov, Pariev & Gabuzda 2004).

A clear spine–sheath polarization structure on parsec scales was observed in the quasar 1055+018 by Attridge, Roberts & Wardle (1999), who interpreted this structure as evidence of a series of shocks in the jet, with a longitudinal ***B*** field at the edges of the jet induced by an interaction with the surrounding medium. However, as we note above, this type of polarization structure could also arise if there is a helical ***B*** associated with the jet.

We report results here for several BL Lac objects displaying such polarization structures in their VLBI jets, including 1652+398, whose 'spine–sheath' polarization structure was first described by Aaron (1996) in his thesis. We present and discuss our multifrequency Very Long Baseline Array (VLBA) total intensity and polarization images of these sources here, together with new ground- and space-VLBI observations of one of these objects and of 1055+018. These images demonstrate that spine–sheath polarization structures are not uncommon among blazars, but the most likely origin of these structures is not entirely clear.

⋆E-mail: contour@mail.ru

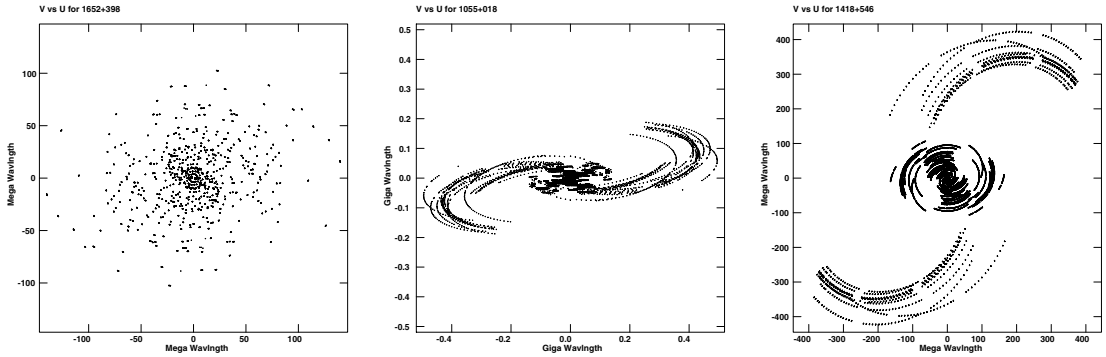

Figure 1. Coverages of the u–v plane at 5 GHz for VLBA observations of 1652+398 at epoch 1997.11 (left), VSOP observations of 1055+018 at epoch 1999.36 (middle) and VSOP observations of 1418+546 at epoch 2001.46 (right).

2 OBSERVATIONS

2.1 5-GHz global VLBI observations, epoch 1995.41

The source 1418+546 was observed together with a number of other BL Lac objects at 5 GHz over 24 h starting at 16.00 UT on 1995 May 30 using a global array consisting of the Medicina (32 m), Effelsberg (100 m), St. Croix (25 m, VLBA), Hancock (25 m, VLBA), Green Bank (43 m), North Liberty (25 m, VLBA), Owens Valley (40 m), Brewster (25 m, VLBA), and Mauna Kea (25 m, VLBA) antennas and the Westerbork phased array ($\sqrt{14} \times 25$ m). The observations were made under the auspices of the US and European VLBI networks. The data were recorded using the MkIII system and correlated at the MkIII correlator at the Max-Planck-Institut für Radioastronomie in Bonn. All antennas recorded both right- and left-circular polarizations (RCP and LCP) except for Medicina, which recorded only LCP. The data reduction and imaging were done in the Brandeis VLBI package (Roberts, Wardle & Brown 1994).

The strong source 3C84, which has a complex intensity structure but is essentially unpolarized at 5 GHz, was used to determine the instrumental polarizations ('D-terms') of each antenna. The absolute orientation of the polarization electric vector position angles (EVPA) was calibrated using VLBI observations of several compact, polarized sources together with measurements of their integrated polarization from data obtained at 5 GHz at the University of Michigan Radio Astronomy Observatory a few days later (on June 3–5). We estimate the resulting uncertainty in the absolute χ values to be 4–5°.

2.2 Multifrequency VLBA observations, epoch 1997.11

Observations of 24 BL Lac objects, including 0745+241, 1418+546 and 1652+398 were made on 1997 February 9 using the National Radio Astronomy Observatory (NRAO) VLBA[1] of ten 25-m antennas: St. Croix; Hancock; North Liberty; Fort Davis; Los Alamos; Pietown; Kitt Peak; Owens Valley; Brewster; and Mauna Kea. The observations were carried out at 15, 8.4 and 5 GHz with full polarization sensitivity. The data were correlated at the VLBA correlator in Socorro, New Mexico and were calibrated and imaged in the NRAO AIPS package using standard techniques.

The strong unpolarized source 3C84 was used to determine the instrumental polarizations ('D-terms') of each antenna for each frequency. The absolute orientation of the EVPAs was calibrated using VLBA observations of the compact, strongly polarized source 1823+568 together with measurements of its integrated polarization from Very Large Array (VLA) data obtained roughly 1 day after the end of the VLBA run. The resulting uncertainty in the absolute χ values is about 3° at all frequencies. The u–v coverage obtained for 1652+398 at 5 GHz is shown in Fig. 1 (left); the coverage at the other frequencies is virtually identical but scaled accordingly. The u–v coverage obtained for 0745+241 and 1419+546 are qualitatively similar.

[1] The NRAO is a facility of the National Science Foundation operated under cooperative agreement by Associated Universities, Inc.

2.3 1.6 and 5 GHz VSOP observations, epoch 1999.36

VLBI Space Observatory Programme (VSOP) polarization observations of 1055+018 were obtained on 1999 May 12 and 13 at 1.6 and 5 GHz, respectively. Each of the observing sessions lasted 8.5 h. The ground array for the 5-GHz observations included the ten VLBA antennas and the Effelsberg (100 m) telescope, while the ground array for the 1.6-GHz observations included the two 70-m antennas of the Deep Space Network (DSN) at Goldstone and Robledo in addition to these 11 antennas. The resulting u–v coverage at 5 GHz is presented in Fig. 1 (middle); the 1.6-GHz u–v coverage is very similar and scaled accordingly.

All antennas except for the orbiting antenna HALCA and the Goldstone and Robledo antennas observed both RCP and LCP; these three antennas observed only LCP. The data-recording mode was the same as that described by Gabuzda & Gómez (2001). The data were correlated at the VLBA correlator in Soccoro, New Mexico.

The polarization calibration was done using the task LPCAL to find a joint solution for the instrumental polarizations of all antennas and for the source polarization. The instrumental polarizations for all ground antennas were 1–3 per cent; the HALCA instrumental polarizations were both estimated to be 3–4 per cent.

The compact polarized source OJ287 had been observed with the 5-GHz ground array to be used in calibrating the absolute polarization position angles. Unfortunately, no integrated polarization measurements for this source were available very near the VSOP observations. We therefore tentatively applied the same polarization-angle calibration that we had used in VSOP polarization observations carried out in the same mode in 1999 April 4 using the same reference antenna (Gabuzda & Gómez 2001). This calibration yielded a polarization map for OJ287 that is consistent with a 5-GHz University of Michigan Radio Astronomy Observatory integrated polarization measurement obtained on 1999 May 30, two weeks after our VSOP observations. In addition, as is discussed below, the polarization of the jet ridge line in the resulting ground-array polarization image of 1055 + 018 is very similar to the image obtained earlier by Attridge et al. (1999). We estimate that the

uncertainty in the absolute χ calibration is no worse than 10°; while less accurate than we would like, this is sufficient to provide a clear qualitative picture of the ground array and VSOP polarization structure of 1055 + 018.

The polarization angle calibration at 1.6 GHz was complicated by two factors: the lack of integrated polarization measurements at this frequency for any of the sources observed by the ground VLB array and the large influence of even modest Faraday rotation on the observed polarization angles. We therefore adopted the following procedure. We first removed the effect of the integrated (presumed foreground, i.e. Galactic) rotation measure (RM) of 1055 + 018, found by Kim, Tribble & Kronberg (1991) to be -45 rad m^{-2}, by rotating the observed polarization angles in all pixels of the ground-array χ maps for 1055+018 by +10° at 5 GHz and +86.5° at 1.6 GHz. We then determined the rotation necessary at 1.6 GHz to make the polarization angles in an optically thin VLBI jet component at a distance of about 9 mas align with the calibrated polarization angles at 5 GHz. This region was well resolved from the core in the maps at both frequencies, and the linear polarization in this region was clearly detected in both polarization maps. The assumptions made with this procedure are that: (i) the RM at this location was fully accounted for by subtracting the rotation corresponding to the integrated RM of Kim et al. (1991); and (ii) the intrinsic polarization angles at the two frequencies should, in fact, be aligned. It is likely that one or both of these assumptions are not entirely correct, but this approach enabled us to obtain at least an approximate picture of the polarization structure of the source at 1.6 GHz; in addition, even if our overall polarization angle calibration is not correct, the relative angles for polarization in different regions of the source are still correct, so that some information about the polarization structure is retained. We will discuss the conclusions that can be drawn under these conditions below.

2.4 5-GHz VSOP observations, epoch 2001.46

Our VSOP polarization observations of 1418+546 were obtained on 2001 June 18. The observation session lasted 8 h, and the ground array included the ten VLBA antennas and the Effelsberg (100 m) telescope. The resulting u–v coverage is presented in Fig. 1 (right).

All antennas except for the orbiting antenna HALCA observed both RCP and LCP; HALCA observed only LCP. The data-recording mode was the same as that described by Gabuzda & Gómez (2001). The data were calibrated at the VLBA correlator in Soccoro, New Mexico.

The polarization calibration was done using the AIPS task LPCAL to find a joint solution for the instrumental polarizations of all antennas and for the source polarization. The instrumental polarizations for all ground antennas were 1–3 per cent; the HALCA instrumental polarization was estimated to be about 3 per cent. Absolute calibration of the polarization angles χ was performed by comparing the total polarization detected in ground-only VLBI images of the compact, polarized sources OJ287 and 1749+096 with integrated VLA measurements obtained by the NRAO; in both cases, integrated measurements were fortuitously available within 5–8 d both before and after the VSOP observations, and did not show evidence for variability between the integrated measurements. The absolute χ calibration is therefore estimated to be good to within about 4°.

3 RESULTS AND DISCUSSION

The results for the four sources are discussed below. In each of the images, the total intensity contours and plane of the polarization ***E*** vectors are superimposed. The polarization vectors for 1055+018 have been corrected for the integrated Faraday rotation of this source at both 5 and 1.6 GHz, as the 1.6 GHz polarization vectors would be meaningless without such a correction (the rotation corresponding to the integrated Faraday RM of -45 rad m^{-2} is -86.5° at 1.6 GHz). The polarization vectors for the remaining sources have been corrected for their integrated RMs when these corrections are greater than 2°; in all cases, the corresponding corrections are modest: $\leqslant$4.3° for 0745 + 241 (RM = +21 rad m^{-2}; Pushkarev 2001), $\leqslant$3.5° for 1418 + 546 (RM = +17 rad m^{-2}; Rudnick & Jones 1983) and $\leqslant$8.5° for 1652+398 (RM = +42 rad m^{-2}; Rusk 1988). The parsec-scale RM distributions for 0745 + 241 and 1652 + 398 are discussed in more detail by Gabuzda, Murray & Cronin (2004).

Table 1. Source models: 0745+241 (1997.11).

	I (mJy)	r (mas)	Δr (mas)	θ (deg)	$\Delta\theta$ (deg)	MAJ (mas)	p (mJy)	χ (deg)	m (per cent)
					6 cm				
C	326	–	–	–	–	0.06	<1.3		>0.4
J6	70	0.65	0.01	−59	0.9	0.10	12.3	98	17.6
J5	95	2.69	0.01	−64	0.2	0.52	16.3	98	17.2
J4	39	3.60	0.02	−52	0.4	0.55	6.1	29	>15.6
J3	26	6.10	0.06	−50	0.6	1.89	<1.3		<4.9
J2	14	8.20	0.08	−45	0.5	1.08	4.0	34	28.6
J1	6	9.98	0.32	−44	1.9	2.06	<1.3		<21.6
					4 cm				
C	340	–	–	–	–	0.19	<1.0		<0.3
J6	61	0.73	0.01	−62	0.8	0.38	14.4	110	23.6
J5	57	2.82	0.01	−66	0.2	0.56	12.8	93	22.4
J4	32	3.42	0.01	−58	0.3	0.19	2.5	28	>7.8
J3	22	5.58	0.10	−50	1.0	2.14	<1.0		<4.5
J2	13	8.34	0.14	−46	0.9	1.73	3.5	30	26.9
					2 cm				
C	389	–	–	–	–	0.16	8.3	109	2.3
J6	53	0.66	0.03	−66	1.9	0.55	9.0	126	17.0
J5	26	2.96	0.05	−67	0.8	0.18	7.9	86	30.4
J4	33	3.93	0.03	−61	0.9	0.49	<2.2		<6.5

Models for the source structures were derived by model fitting the complex I and P visibilities that come from the mapping process with circular Gaussian components, as described by Roberts, Gabuzda & Wardle (1987) and Gabuzda, Wardle & Roberts (1989). The model fits are shown in Tables 1–4. I and p are the total and polarized fluxes of each component, respectively. The full width at half maximum of the Gaussian components is denoted by MAJ. We denote distance from the core by r and the VLBI jet direction by θ, with Δr and $\Delta\theta$ being the corresponding errors. In all cases, the I and P visibilities were fitted separately, in order to allow for small differences in the positions and sizes of corresponding I and P components, either intrinsic to the source structure or associated with residual calibration errors. We have identified P components with specific I components when their positions agreed to within their errors; for those P components that have significant offset from the nearest I components (toward an edge of the jet) we give a lower limit for the degree of polarization m. The positions given in Tables 1–4 are those for the I models, which we consider to be more accurate. The errors of the separations of jet components from the core are formal 1σ errors, corresponding to an increase in the best-fitting χ^2 by unity. The smallest of these formal errors certainly underestimate the actual errors; realistically, the smallest 1 σ errors are probably no less than 0.03, 0.06, 0.1 and 0.3 mas at 15, 8.4, 5 and 1.6 GHz, respectively.

Table 2. Source models: 1055+018 (1999.36).

	I (mJy)	r (mas)	Δr (mas)	θ (deg)	$\Delta\theta$ (deg)	MAJ (mas)	p (mJy)	χ (deg)	m (per cent)
6 cm VLBA + Effelsberg									
C	1058	–	–	–	–	0.43	11.8	63	1.1
J5	574	1.85	0.01	−48	0.2	0.63	32.0	−69	5.6
J4	548	5.49	0.02	−51	0.2	0.28	21.8	−63	3.9
J3	216	9.24	0.02	−62	0.1	1.92	28.5	88	13.2
J2	8	15.92	0.29	−76	3.9	0.82	<2.0		<25.0
6 cm VLBA + Effelsberg + HALCA									
C	891	–	–	–	–	0.17	<3.5		<0.4
J6	94	0.39	0.01	−29	3.1	0.01	10.4	70	10.4
J5	544	1.76	0.01	−49	0.3	0.56	32.5	−75	6.0
J4.5	145	3.31	0.02	−40	0.3	1.34	<3.5		<2.4
J4	396	6.03	0.01	−50	0.1	1.90	27.0	−65	6.8
J3	273	9.05	0.03	−62	0.2	2.59	30.3	83	11.1
18 cm VLBA + Effelsberg + DSN									
C	648	–	–	–	–	0.20	21.7	−73	3.3
J5	573	2.06	0.02	−49	0.4	0.03	<1.1		<0.2
J4	774	5.59	0.01	−53	0.1	2.61	16.9	−55	2.2
J3	245	8.94	0.01	−64	0.1	0.85	33.5	89	13.6
J2	274	14.17	0.06	−68	0.4	14.83	11.6	39	>4.2
J1	37	32.57	0.25	−50	0.5	8.99	<1.1		<2.9
18 cm VLBA + Effelsberg + DSN + HALCA									
C	372	–	–	–	–	0.47	19.6	−71	5.3
J5	755	1.70	0.01	−49	0.2	0.67	<4.0		<0.5
J4	657	5.35	0.01	−51	0.1	2.02	14.7	−53	2.2
J3	470	8.59	0.01	−63	0.1	3.01	29.6	88	6.3
J2	67	15.76	0.08	−71	0.8	4.67	5.5	31	>8.2
J1	26	21.08	0.24	−64	1.3	2.21	<4.0		<15.4

Throughout this paper, the values $H_0 = 70\,\mathrm{h\,km\,s^{-1}\,Mpc^{-1}}$, $q_0 = 0.05$ and $S \propto \nu^{+\alpha}$ will be used. The choice of cosmological model is relevant only in connection with determining the superluminal speeds implied by the observed proper motions in 1055+018; we have adopted the same model as Attridge et al. (1999) to facilitate comparison with their results.

3.1 0745+241

This object was identified as a BL Lac candidate owing to its featureless optical spectrum (Wilkes et al. 1983). Later spectroscopic observations detected [O II] λ3727 and [O III] λλ4959, 5007 emission lines at a redshift of $z = 0.41$ (Stickel, Fried & Kühr 1989). Kiloparsec-scale radio images of 0745+241 taken by Murphy, Browne & Perley (1993) and Perley (1982) show a classical triple structure with a core and two lobes separated by ≃15 arcsec.

In our earlier 5-GHz global VLBI observations (Gabuzda, Pushkarev & Cawthorne 1999), the orientation of the observed polarization vectors in the inner jet seemed to have no obvious relation to the local jet direction, while the polarization in the outer jet was oriented transverse to the jet, implying a longitudinal $\boldsymbol{B}$ field in the case of optically thin emission. Our multifrequency VLBA observations (Fig. 2) have revealed the magnetic-field structure of the source much more clearly: in the innermost polarized components detected at 15 GHz, the inferred $\boldsymbol{B}$ field is orthogonal to the jet axis (polarization aligned with the jet; Fig. 2, top), while further from the core it becomes nearly longitudinal (Fig. 2, middle and bottom). The polarization in the outer jet is also offset to the north from the main total intensity ridge line of the jet, bringing to mind a possible interaction with a surrounding medium.

Table 3. Source models: 1418+546.

	I (mJy)	r (mas)	Δr (mas)	θ (deg)	$\Delta\theta$ (deg)	MAJ (mas)	p (mJy)	χ (deg)	m (per cent)
1997.11									
6 cm									
C	547	–	–	–	–	0.20	4.5	92	0.8
J6	133	1.29	0.01	131	0.4	0.54	5.7	23	4.3
J5	58	5.03	0.04	126	0.5	2.13	2.9	89	>5.0
J4	17	7.77	0.28	126	2.1	3.91	<0.9		<5.3
J3	11	12.46	0.36	134	1.7	3.44	<0.9		<8.3
J2	22	16.28	0.23	120	0.9	4.33	<0.9		<4.1
J1	22	20.25	0.36	125	1.0	5.65	<0.9		<4.1
4 cm									
C	586	–	–	–	–	0.19	4.7	37	0.8
J6	122	1.26	0.01	132	0.2	0.59	3.7	19	>3.0
J5	54	5.15	0.05	127	0.5	2.58	<1.2		<2.2
J3	37	13.57	0.29	123	0.9	6.76	<1.2		<3.2
2 cm									
C	602	–	–	–	–	0.16	14.7	89.4	2.4
J6	99	1.32	0.01	132	0.4	0.48	<3.2		<3.2
J5	10	5.40	0.03	131	0.4	0.11	<3.2		<32.2
2001.46									
6 cm VLBA + Effelsberg									
C	525	–	–	–	–	0.09	<0.3		<0.1
J7	184	0.59	0.02	131	1.3	0.45	12.5	58	6.8
J6	88	1.51	0.01	125	0.2	0.40	3.0	132	3.4
J5	24	4.13	0.03	131	0.4	1.41	1.7	45	7.1
J3	5	13.34	0.43	136	1.9	1.25	<0.3		<6.0
J2	29	15.93	0.35	121	1.0	4.27	2.9	97	10.0
J1	35	19.05	0.46	125	1.0	6.18	0.9	109	2.6
6 cm VLBA + Effelsberg + HALCA									
C	423	–	–	–	–	0.16	<1.0		<0.2
J7	202	0.31	0.01	151	1.3	0.35	14.9	73	7.3
J6a	111	1.03	0.01	126	0.3	0.41	4.5	15	>4.0
J6a	49	1.71	0.01	128	0.4	0.48	3.7	134	7.5
J5	22	4.20	0.07	130	0.8	1.48	<1.0		<4.5

We were able to identify a number of VLBI components in the maps at two or more of the three frequencies, enabling us to estimate spectral indices between 8.4 and 15 GHz and 5 and 8.4 GHz for the core and several jet components (Table 5). The core is partly optically thick ($\alpha \simeq 0$ to $+0.2$), while the jet components are primarily optically thin, as expected ($\alpha \simeq -0.2$ to -1.3).

3.2 1055+018

1055+015 ($z = 0.889$) is a stongly variable radio source with a relatively flat spectrum, classified as a blazar by Impey & Tapia (1990). The optical spectrum of the source shows several emission lines with relatively small rest-frame equivalent widths (Falomo, Scarpa & Bersanelli 1994; Appenzeller et al. 1998): $W_{\rm eq}$([C III] λ1909) ≃ 8 Å, $W_{\rm eq}$([Mg II] λ2798) ≃5–17 Å. On kiloparsec scales, this object has a bright core and two lobes with a jet extending up to 30 arcsec toward the southern lobe, which lies in position angle 180° (Murphy et al. 1993). The parsec-scale structure at 43 GHz investigated by Lister, Marscher & Gear (1998) showed a 2-mas jet in position angle −63° near the core ($r = 0.23$ mas) and −46° further out ($r = 1.95$ mas). Polarization observations at 5 GHz (epoch 1997.07) revealed an intriguing structure in both total intensity and polarization, suggesting the presence of a fragmentary boundary layer

Table 4. Source models: 1652+398 (1997.11).

	I (mJy)	r (mas)	Δr (mas)	θ (deg)	$\Delta\theta$ (deg)	MAJ (mas)	p (mJy)	χ (deg)	m (per cent)
					6 cm				
C	461	–	–	–	–	0.28	<1.3		<0.3
J5	114	1.16	0.02	153	0.6	0.77	<1.3		<1.1
J4	184	3.02	0.01	147	0.2	0.95	20.7	26	>11.5
J3	82	4.02	0.03	124	0.4	1.43	14.4	6	>16.9
J2	143	7.47	0.04	114	0.3	3.17	11.3	100	>7.9
J0	69	19.04	0.65	122	1.8	12.11	>1.3		<1.9
					4 cm				
C	417	–	–	–	–	0.25	<1.0		<0.8
J5	112	0.96	0.01	156	0.6	0.77	4.3	17	2.5
J4	170	3.07	0.01	148	0.1	1.19	4.1	21	>6.9
J3	59	4.11	0.03	125	0.5	1.25	13.8	18	>23.4
J2	113	7.46	0.06	113	0.5	2.85	7.4	102	6.5
J1	10	9.58	0.41	129	2.2	1.81	<1.0		<10.0
					2 cm				
C	355	–	–	–	–	0.14	7.9	154	2.2
J5	103	0.72	0.01	161	0.8	0.69	5.8	161	5.6
J4	138	3.16	0.02	147	0.4	1.29	4.3	34	3.1
J3	44	4.38	0.06	125	0.9	1.38	5.1	30	>11.6
J2	72	7.65	0.07	111	0.6	2.36	<2.3		<3.1

where the magnetic field was predominantly parallel to the jet axis (Attridge et al. 1999).

Fig. 3 presents I and p images of 1055+018 obtained at 1.6 and 5 GHz using the ground antennas only. The 5-GHz ground-based images (Fig. 3, top) show that the source has changed appreciably since epoch 1997.07 (Attridge et al. 1999): the peak I and p flux densities have both decreased by about 40 per cent. The polarization structure along the jet 'spine' is remarkably similar to that shown in fig. 2 of Attridge et al. (1999), with the inferred spine $\boldsymbol{B}$ field being perpendicular to the local jet direction. The 'sheath' is also visible in both our I and p images.

Our beam was somewhat smaller than that of Attridge et al. (1999), owing primarily to the fact that our array included the Effelsberg antenna, while the array of Attridge et al. (1999) included one antenna of the VLA. This relatively modest increase in resolution reveals a tentative detection of interknot polarization between the features we have labelled J4 and J3 (Fig. 3, top right), with its χ vectors well aligned with the local jet direction. This argues in support of the transverse jet-spine $\boldsymbol{B}$ field being associated with a dominant toroidal field component, rather than a series of shocks in the VLBI jet.

To compare our 5-GHz polarization image with that of Attridge et al. (1999), we made a polarized-flux image with the same beam size and contour levels in mJy and with the observed χ vectors rotated by 90° as in fig. 2 of Attridge et al. (1999), shown in Fig. 4. The close similarity between the two images is striking. The fact that the jet polarization structures at the two epochs agree so well in a number of details reassures us that the absolute calibration of the 5-GHz polarization position angles is good to within a few degrees – for example, both 5-GHz polarization images show a transition from a region with polarization $\boldsymbol{E}$ vectors oriented at −45° to $\boldsymbol{E}$ oriented at 90° 5–10 mas from the core. The sheath polarization structures are also similar, though there may have been some redistribution in the sheath polarized flux between the two epochs. There appears to have been a modest but significant rotation in the VLBI core between the two epochs.

Fig. 5 presents the images of 1055+018 obtained at 1.6 and 5 GHz using the whole array, including the orbiting telescope. The VSOP map of 1055+018 at 5 GHz (Fig. 5, top) displays the structure of the source in more detail. The interknot polarization that is shown by our ground-array p image is largely resolved out, though traces of it remain in the VSOP p image; the sheath emission is likewise nearly completely resolved out. The extra resolution provided by the space–ground baselines enabled us to separate the ground-based core into two components – a bright but weakly polarized core and the inner-jet component J6, which is polarized about 10 per cent. We were able to infer the presence of this comparatively weak component in part because the polarized emission near the VSOP core was coincident with the inner jet rather than the VSOP core itself. A number of BL Lac objects that have been observed with VSOP have likewise been found to have their ground-based core polarizations dominated by the contribution of inner-jet components (Gabuzda 1999; Gabuzda & Gómez 2001; Gabuzda 2003).

Both the ground-based and the VSOP images at 1.6 GHz (Figs 3 and 5, bottom) clearly show the sheath of polarization roughly 10–20 mas from the core offset to the south from the main total intensity ridge line. Despite the assumptions we have had to adopt in our absolute calibration of the 1.6-GHz polarization angles, the distributions of the χ vectors in the 5-GHz ground p image (Fig. 3, top right) and the 1.6-GHz VSOP p image (Fig. 5, bottom right) are in excellent agreement (as they should be, as we have taken out the effects of the Galactic RM at both frequencies).

We used the 5-GHz ground-based and 1.6-GHz VSOP polarization-angle maps to construct a two-frequency RM distribution for 1055+018 (Fig. 6, right). As the effect of the integrated Faraday rotation was subtracted before comparing the polarization angles, these 'residual' RMs should reflect the distribution of thermal gas in the vicinity of the AGN. Despite any uncertainties in this RM distribution, it does accurately reflect the RMs of particular regions relative to other regions. The fact that the RM is close to zero in the VLBI jet about 9 mas from the core is a direct consequence of the procedure we adopted to calibrate the 1.6-GHz polarization angles. We can see that this calibration also yields RMs no larger in magnitude than about 10 rad m^{-2} throughout the central region of the jet, from roughly 2–10 mas from the core, with a slightly higher RM being implied for the southern sheath emission. We can also see that the RM distribution is non-uniform (i.e. there is no single rotation that could be applied to all the angles at 1.6 GHz to make them all align with the angles at 5 GHz), possibly owing to non-uniformity in the thermal plasma in the immediate vicinity of 1055 + 018. The large difference in the observed core polarization angles at 1.6 and 5 GHz appears here as an increase in the inferred RM toward the core.

We determined the 5–1.6 GHz spectral indices of the core and four jet components using the fluxes from the 1.6-GHz VSOP model and the 5-GHz ground-array model, for which the corresponding visibility data have comparable resolutions (Table 5). The core is optically thick, with a rather inverted spectrum ($\alpha = +0.97$). Table 2 shows that the nominal difference in the observed polarization angles at 1.6 and 5 GHz is about 45°; given the large positive spectral index between these frequencies, it is likely that this includes a 90° rotation owing to the optically thick–thin transition, which likely occurs between 1.6 and 5 GHz. However, as the effect of Faraday rotation is large at 1.6 GHz, this difference in the polarization angles could also be associated entirely or partly with a modest enhancement of the RM of the core region compared to the jet region we used to perform our polarization angle calibration at 1.6 GHz (an RM of about 23 rad m^{-2} would give rise to a rotation of about 55°).

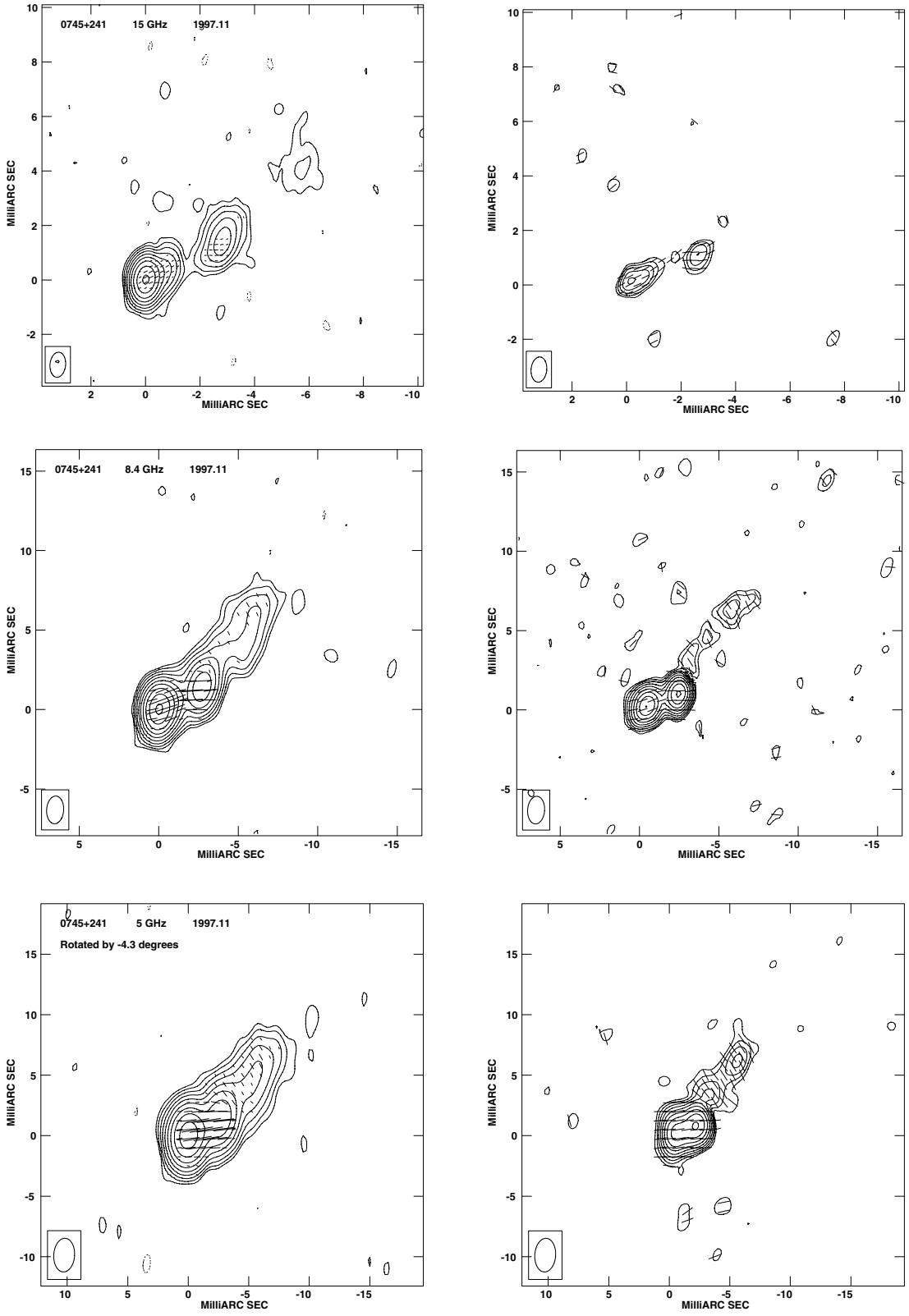

Figure 2. Left: *I* images of 0745+241 at epoch 1997.11 with contours increasing in steps of two and *P* vectors superimposed. Right: corresponding polarized flux images with contours increasing in steps of $\sqrt{2}$ and χ vectors superimposed. Top: 15 GHz, bottom *I* contours at ± 0.35 per cent of the peak brightness of 378 mJy beam^{-1}; bottom *p* contour at 24 per cent of the peak brightness of 9.0 mJy beam^{-1}. Middle: 8.4 GHz, bottom *I* contours at ± 0.175 per cent of the peak brightness of 354 mJy beam^{-1}; bottom *p* contour at 6 per cent of the peak brightness of 12.1 mJy beam^{-1}. Bottom: 5 GHz, bottom *I* contours at ± 0.25 per cent of the peak brightness of 370 mJy beam^{-1}; bottom *p* contour at 6 per cent of the peak brightness of 16.2 mJy beam^{-1}.

Table 5. Spectral indices of VLBI components.

	0745+241			1055+018	
	α_{5-8}	α_{8-15}			$\alpha_{1.6-5}$
C	+0.02	+0.23		C	+0.97
J6	−0.22	−0.23		J5	−0.25
J5	−0.83	−1.33		J4	−0.17
J4	−0.37	+0.07		J3	−0.72
J3	−0.28	—		J2	−1.97
	1418+546			1652+398	
	α_{5-8}	α_{8-15}		α_{5-8}	α_{8-15}
C	+0.13	+0.05	C	−0.19	−0.27
J6	−0.16	−0.35	J5	−0.03	−0.14
J5	−0.14	−2.80	J4	−0.14	−0.35
			J3	−0.65	−0.48
			J2	−0.45	−0.74

We can see in Table 5 that the spectra of the jet components tend to gradually become steeper with distance from the core. The spectral-index map made using the 1.6-GHz VSOP and 5-GHz ground images (Fig. 6, left) shows that the spectrum flattens toward the edges of the jet, especially the southern edge, in the region of the polarization sheath.

Our models for 1055+018 are presented in Table 2. Using the 5-GHz models obtained by Attridge et al. (1999) for epochs 1996.02 and 1997.07 together with our results (model for 5-GHz ground-based data), we estimated proper motions of three components (Fig. 7): $\mu = 0.083 \pm 0.056$ mas yr^{-1} ($\beta_{app} = (3.7 \pm 2.5)h^{-1}$) for J5 [C3 in Attridge et al. (1999)], $\mu = 0.071 \pm 0.011$ mas yr^{-1} ($\beta_{app} = (3.2 \pm 0.5)h^{-1}$) for J4 [C2 in Attridge et al. (1999)], and $\mu = 0.029 \pm 0.036$ mas yr^{-1} ($\beta_{app} = (1.3 \pm 1.6)h^{-1}$) for J3 [C1 in Attridge et al. (1999)]. Attridge et al. (1999) did not detect any motion in components J3 or J4 over the roughly 1 yr separating their epochs. We likewise find the speed of J3 to be zero within the

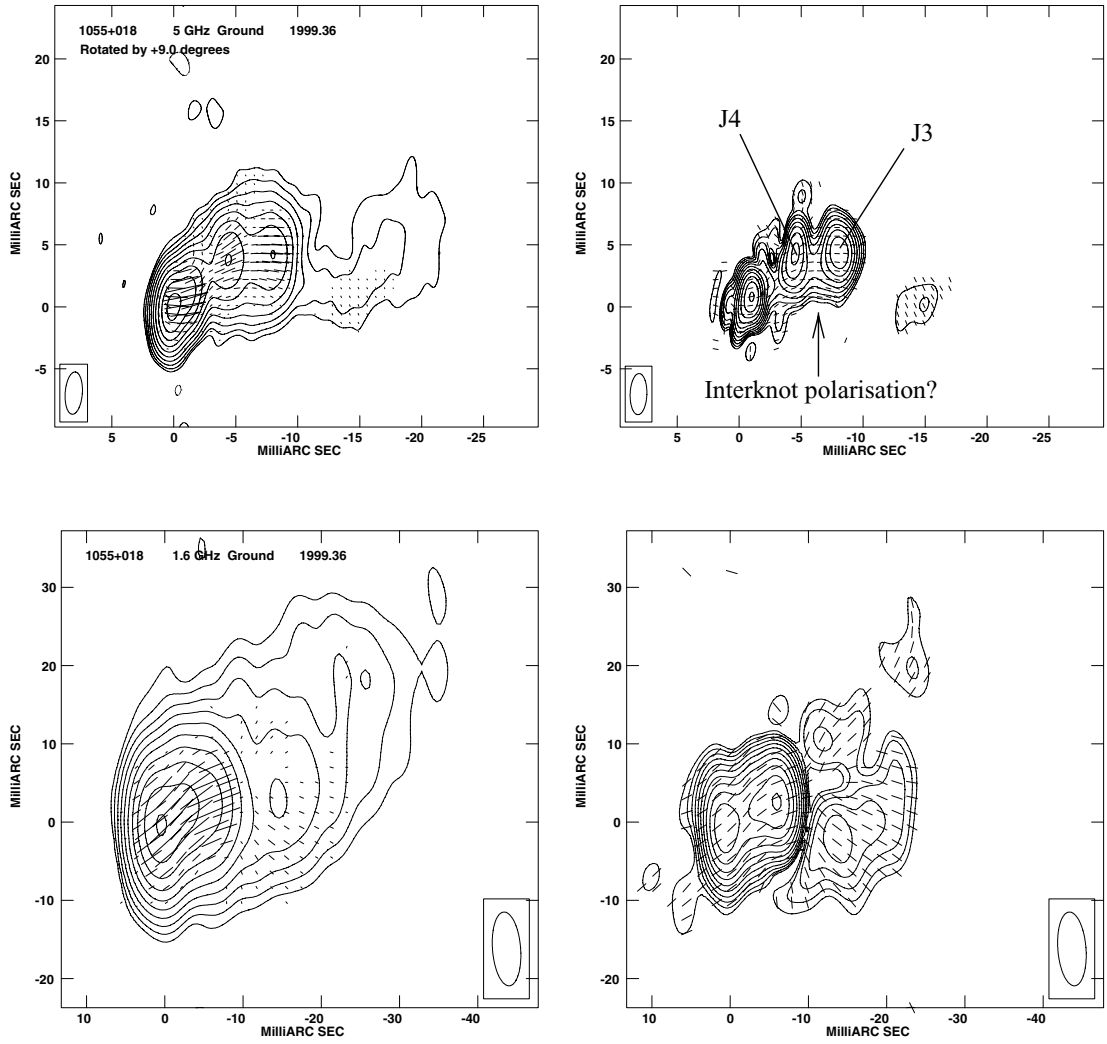

Figure 3. Left: *I* ground-array images of 1055+018 at epoch 1999.36 with contours increasing in steps of two and *P* vectors superimposed. Right: corresponding polarized flux images with contours increasing in steps of $\sqrt{2}$ and χ vectors superimposed. Top: 5 GHz, bottom *I* contours at ±0.15 per cent of the peak brightness of 1054 mJy beam^{-1}; bottom *p* contour at 3 per cent of the peak brightness of 37.8 mJy beam^{-1}. The *p* peaks corresponding to components J3 and J4 are indicated, together with polarization between them that may represent interknot polarization. Bottom: 1.6 GHz, bottom *I* contours at ±0.2 per cent of the peak brightness of 1123 mJy beam^{-1}, with an extra contour at 95 per cent added; bottom *p* contour at 3 per cent of the peak brightness of 34.8 mJy beam^{-1}.

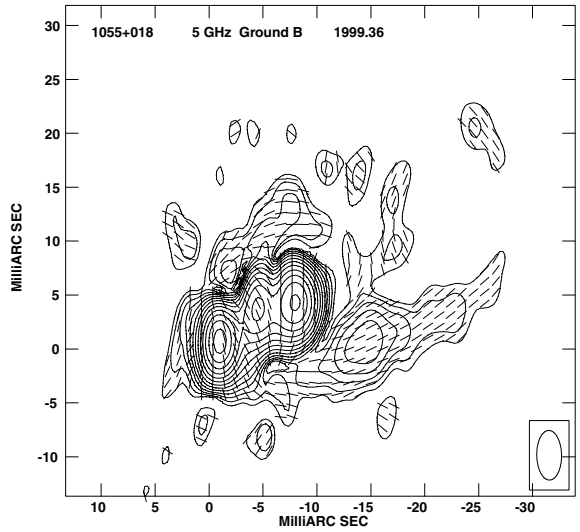

Figure 4. 5-GHz Polarized flux ground-array image for 1055+018 at epoch 1999.36 constructed using the same beam and the same contour levels in mJy as Attridge et al. (1999). The superposed sticks show the χ vectors rotated by 90°, as in fig. 1(b) of Attridge et al. (1999), to depict the inferred direction of the $\boldsymbol{B}$ field.

estimated errors, but the increase in the time baseline between the epochs of Attridge et al. (1999) and our own data yields a non-zero but modest speed for J4. Our nominal speed for J5 is appreciably lower than the estimate of Attridge et al. (1999) [$\beta_{app} = (12 \pm 4.5)h^{-1}$]; this is most likely owing to the relatively large uncertainties in the data requiring a longer time baseline to yield a reliable speed estimate. Thus, overall, the observed component motions indicate an absence of rapid structural variations in 1055+018 between 1996 January and 1999 May.

3.3 1418+546

This BL Lac object is in the centre of a relatively nearby galaxy; the surface brightness profile resembles that of as S0 galaxy, giving rise to speculation that 1418 + 546 could be one of a minority of BL Lac objects with spiral host galaxies (Wurtz, Stoke & Yee 1996). The redshift of $z = 0.152$ reported by Stickel, Fried & Kühr (1993) was based on absorption features of the galaxy, as well as on [O II] λ 3727 and [O III] $\lambda\lambda$ 4959, 5007 emission lines, and confirms the tentative value reported by Stickel et al. (1989).

Fig. 8 shows VLBA images of 1418+546 at 15 (top), 8.4 (middle) and 5 GHz (bottom) for epoch 1997 February. It is clearly visible in the 8.4 and 5 GHz images that the jet polarization is shifted from the

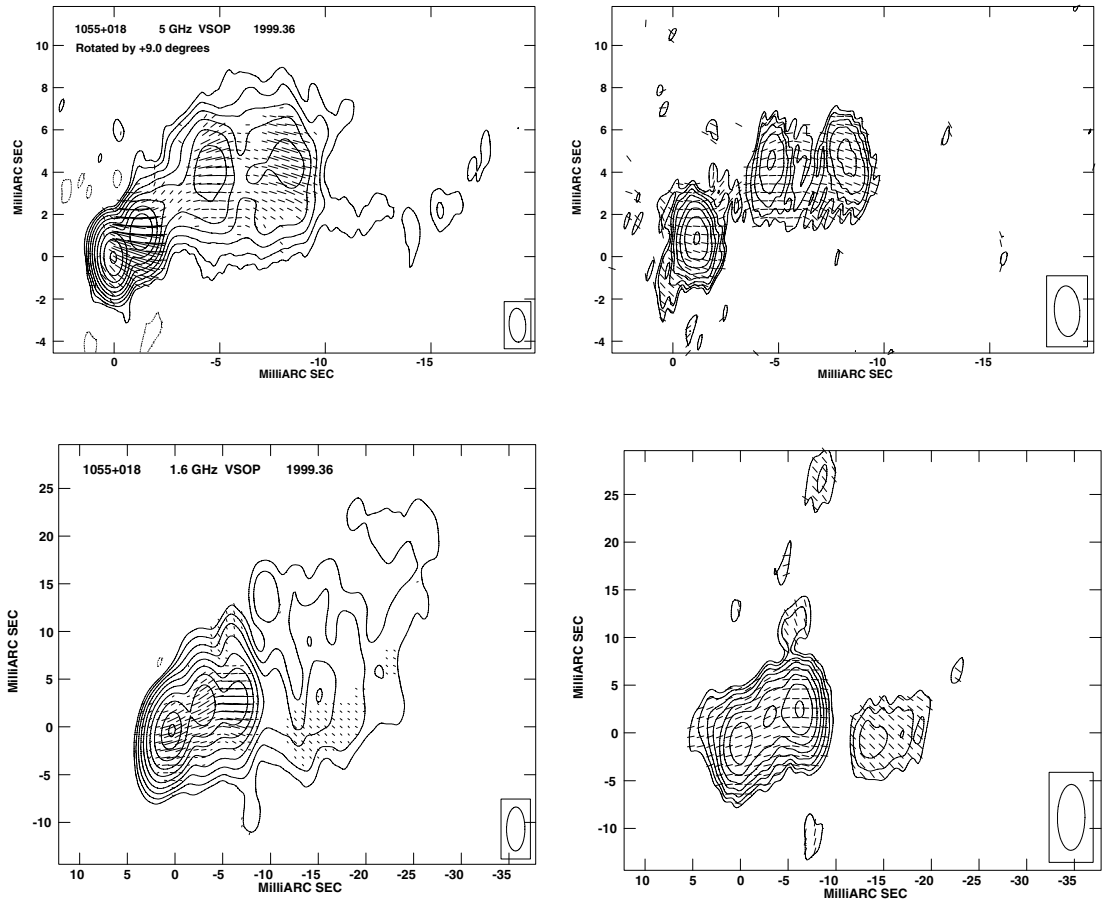

Figure 5. Left: *I* VSOP images of 1055+018 at epoch 1999.36 with contours increasing in steps of two and *P* vectors superimposed. Right: corresponding polarized flux images with contours increasing in steps of $\sqrt{2}$ and χ vectors superimposed. Top: 5 GHz, bottom *I* contours at ±0.18 per cent of the peak brightness of 927 mJy beam^{-1}; bottom *p* contour at 8.5 per cent of the peak brightness of 22.1 mJy beam^{-1}. Bottom: 1.6 GHz, bottom *I* contours at ±0.25 per cent of the peak brightness of 864 mJy beam^{-1}; bottom *p* contour at 8.5 per cent of the peak brightness of 22.0 mJy beam^{-1}.

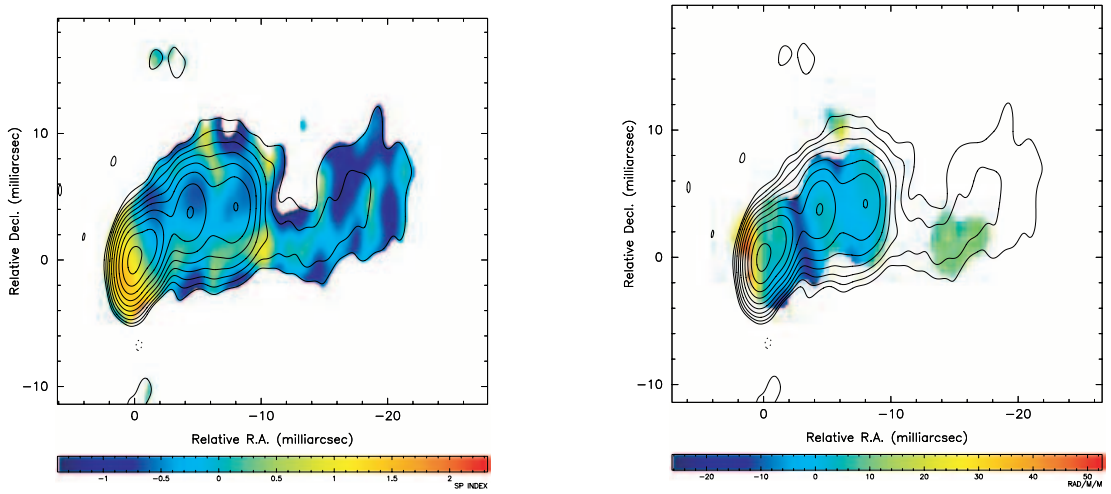

Figure 6. *I* ground-array images of 1055+018 at 5 GHz at epoch 1999.36 from Fig. 3 with the spectral index distribution calculated between 1.6 and 5 GHz (left) and the RM distribution (right) calculated from the 1.6-GHz VSOP and 5-GHz ground-based polarization maps superimposed.

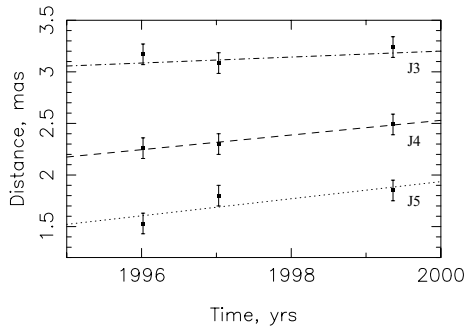

Figure 7. Component motions in 1055+018 at 5 GHz. The distances from the core of the J4 and J3 components have been reduced by 3 and 6 mas, respectively.

jet ridge line toward the southern edge of the jet. However, the 5-GHz image for 1995 May (Fig. 9, top) shows that the jet polarization is shifted toward the *north* from the jet axis at that epoch. In both cases, the observed polarization is roughly orthogonal to the jet direction, implying a predominantly longitudinal magnetic field, as was observed 3 yr earlier by Gabuzda et al. (1999).

In the 5-GHz ground-array image for our VSOP observations (Fig. 9, middle) polarization is detected both in the inner part of the VLBI jet and further from the core. In this case, the jet polarization is reasonably well centred on the jet ridge line, but we can see another curious feature: the polarization vectors alternate in the inner jet from being orthogonal to the jet in the core, to aligned with the jet, then again orthogonal to the jet. One possible origin for this behaviour is the combination of an underlying magnetic field with a net longitudinal component superposed by individual shocks that enhance the local transverse field component, as has been suggested, for example, by Wardle et al. (1994). However, we believe this pattern of alternating orthogonal and longitudinal fields is suggestive that we are observing some sort of global $\boldsymbol{B}$ field associated with the jet, rather than a collection of $\boldsymbol{B}$ fields owing to independent local phenomena.

The full-resolution VSOP image (Fig. 9, bottom) shows that, although the aligned polarization vectors in the inner jet are well centred on the jet ridge line, the orthogonal polarization closer to the core is, in fact, offset toward the southern edge of the jet; note the similarity between this image and the slightly lower-resolution 8.4-GHz VLBA image in Fig. 8 (middle). The VSOP image also demonstrates that the polarization that would be ascribed to the core of the ground-array image is actually dominated by polarized emission from the inner jet, as is typical of other BL Lac objects that have been observed with VSOP (Gabuzda 1999; Gabuzda & Gómez 2001; Gabuzda 2003).

3.4 1652+398

1652+398 (Mkn 501) was discovered during survey observations made by Markarian & Lipovetskii (1974). The optical spectrum of Mkn 501 shows two emission lines, which were identified with [Hα] λ6563 and [N II] λ6584 at a redshift of $z = 0.033$ (Stickel et al. 1993). Mkn 501 was the first object to be discovered as a TeV γ-ray source from the ground (Quinn et al. 1996).

The object has a very rich total intensity structure at 5 GHz (Fig. 10, bottom). The jet propagates about 25 mas ($\sim$16 pc) to the south-east, then turns to the north, rapidly expanding and becoming diffuse. In deep images, a weak cone of emission can be traced tens of milliarcseconds to the northeast (Giroletti et al. 2004).

The polarization structure in the inner 10 mas of the jet is traced well by our VLBA images. The 15-GHz map (Fig. 10, top left) shows polarization associated with the innermost jet and the core, where the polarization is well aligned with the inner jet; however, polarization detected further from the core is offset toward both the northern and southern edges of the jet, with the polarization becoming orthogonal to the jet direction, as was first noted by Aaron (1996, 1999). The polarization structure at 8.4 (Fig. 10, top right) and 5 GHz (Fig. 10, bottom left) shows how this transverse polarization structure develops further from the core. If the observed $\boldsymbol{B}$ field is orthogonal to the observed polarization vectors, the $\boldsymbol{B}$ field is transverse in the central part of the jet and longitudinal at both edges of the jet. To our knowledge, this is the only known case of such a symmetrical 'spine–sheath' polarization structure. It is also noteworthy that the degree of polarization increases toward the edges of the jet (Fig. 11).

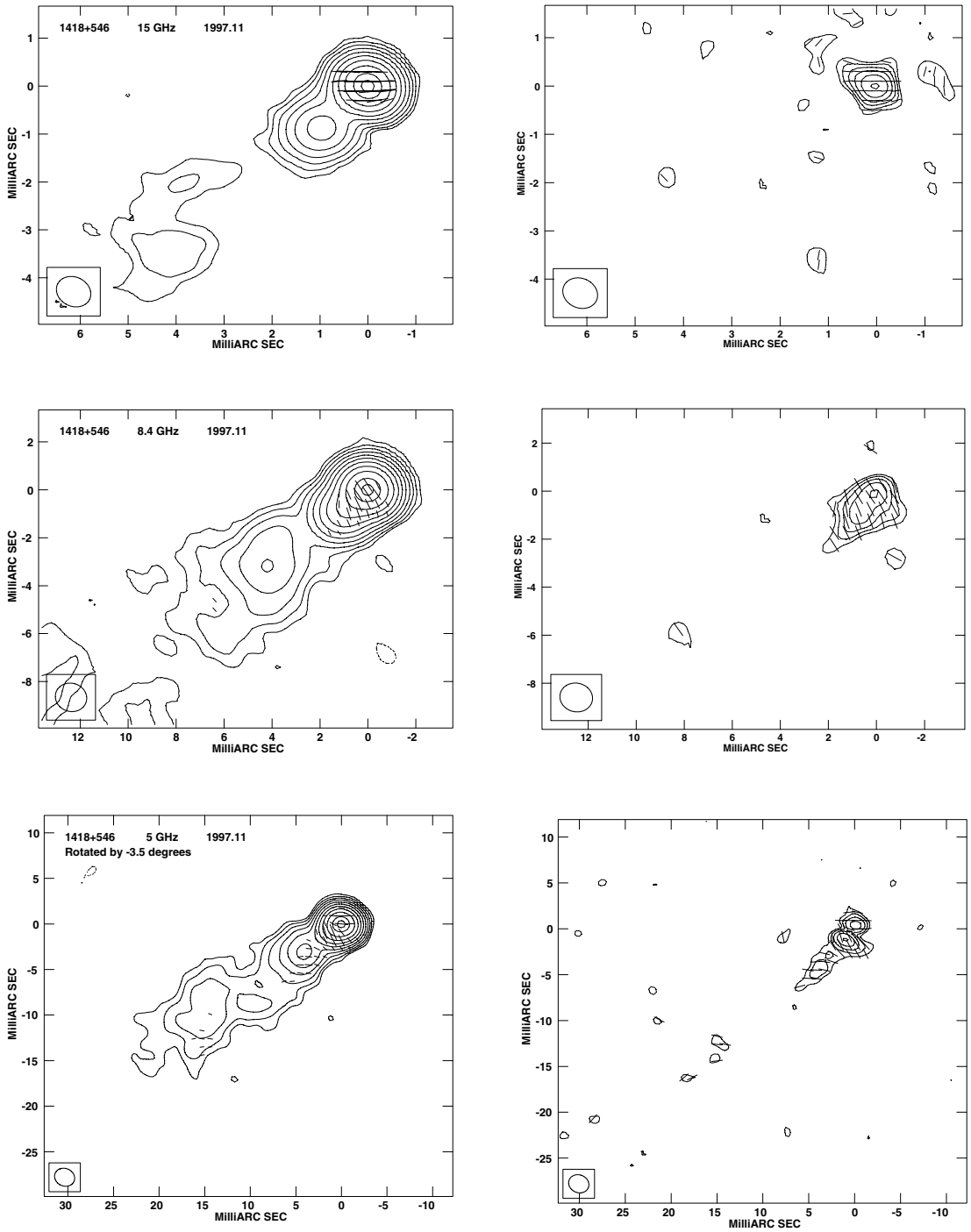

Figure 8. Left: *I* images of 1418+546 at epoch 1997.11 with contours increasing in steps of two and *P* vectors superimposed. Right: corresponding polarized flux images with contours increasing in steps of $\sqrt{2}$ and χ vectors superimposed. Top: 15 GHz, bottom *I* contours at ± 0.25 per cent of the peak brightness of 565 mJy beam^{-1}; bottom *p* contour at 17 per cent of the peak brightness of 13.4 mJy beam^{-1}. Middle: 8.4 GHz, bottom *I* contours at ± 0.125 per cent of the peak brightness of 584 mJy beam^{-1}; bottom *p* contour at 24 per cent of the peak brightness of 4.8 mJy beam^{-1}. Bottom: 5 GHz, bottom *I* contours at ± 0.125 per cent of the peak brightness of 583 mJy beam^{-1}; bottom *p* contour at 24 per cent of the peak brightness of 4.0 mJy beam^{-1}.

4 CONCLUSION

The polarization structure detected in the blazar 1055+018 by Attridge et al. (1999) was striking and provided a clear example of a spine–sheath polarization structure. However, it was not clear how common this type of structure was, as this was the only such case reported in a refereed journal. We have found several BL Lac objects that possess similar polarization structures in their VLBI jets. In all cases, if the ***B*** field is orthogonal to the observed polarization vectors, the ***B*** field is transverse to the jet near the central ridge line and roughly longitudinal at the edges of the jet. These regions of longitudinal field sometimes became detectable only at some distance from the core, often in more extended regions of the jet.

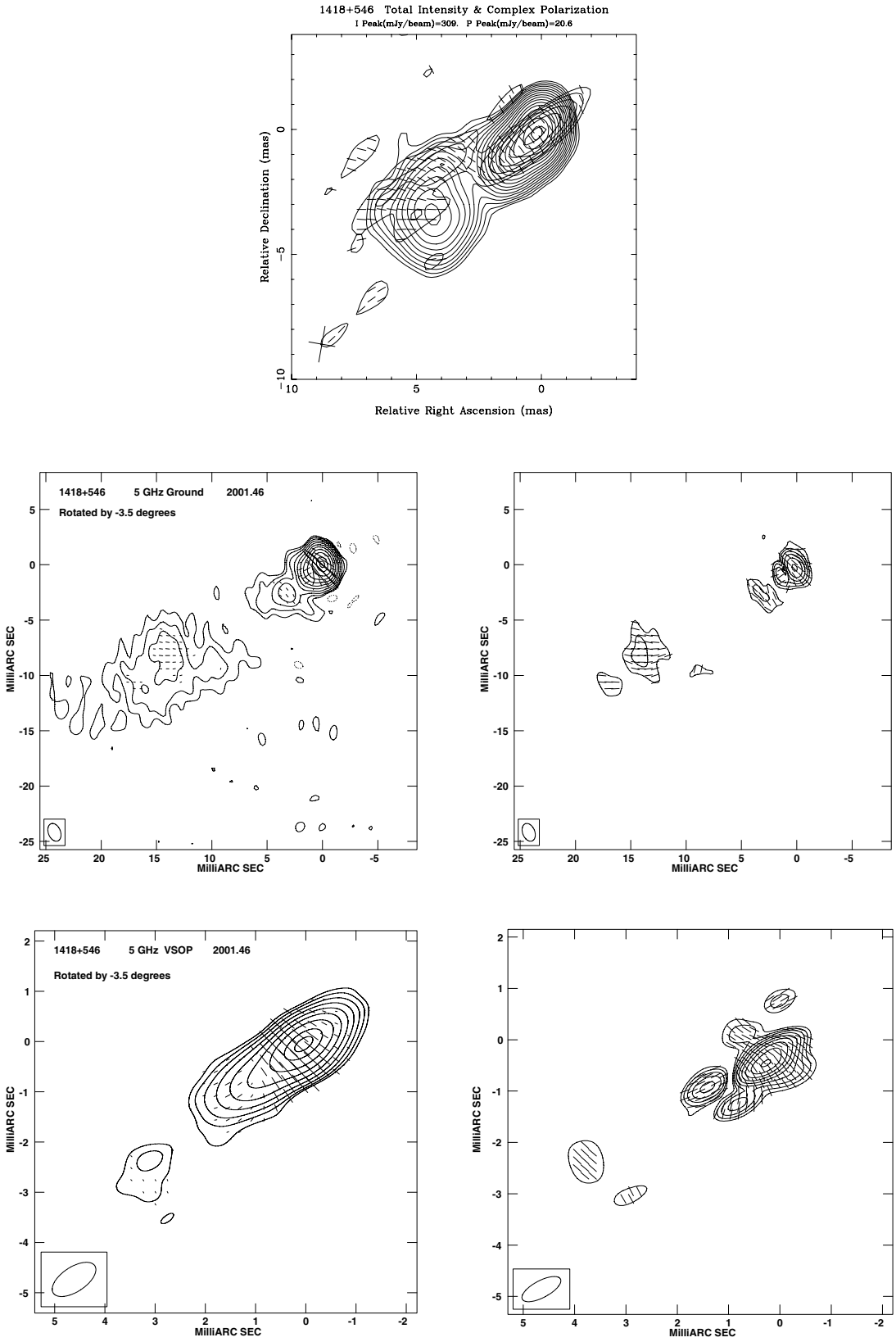

Figure 9. VLBI images of 1418+546 at 5 GHz, with I contours increasing in steps of two and p contours increasing in steps of $\sqrt{2}$. Top: global I image for epoch 1995.41 (light contours) with bottom I contours at ± 0.5 per cent of the peak brightness of 309 mJy beam^{-1} and superposed bold p image with bottom contour at 16 per cent of the peak polarized flux of 20.6 mJy beam^{-1}. Middle: ground-array I image for epoch 2001.46 with bottom contours at ± 0.125 per cent of the peak brightness of 623 mJy beam^{-1} (left); corresponding p image with bottom contour at 2.8 per cent of the peak brightness of 12.0 mJy beam^{-1}. Bottom: VSOP I image for epoch 2001.46 with bottom contours at ± 0.5 per cent of the peak brightness of 485 mJy beam^{-1}; corresponding p image with bottom contour at 6 per cent of the peak brightness of 9.3 mJy beam^{-1}.

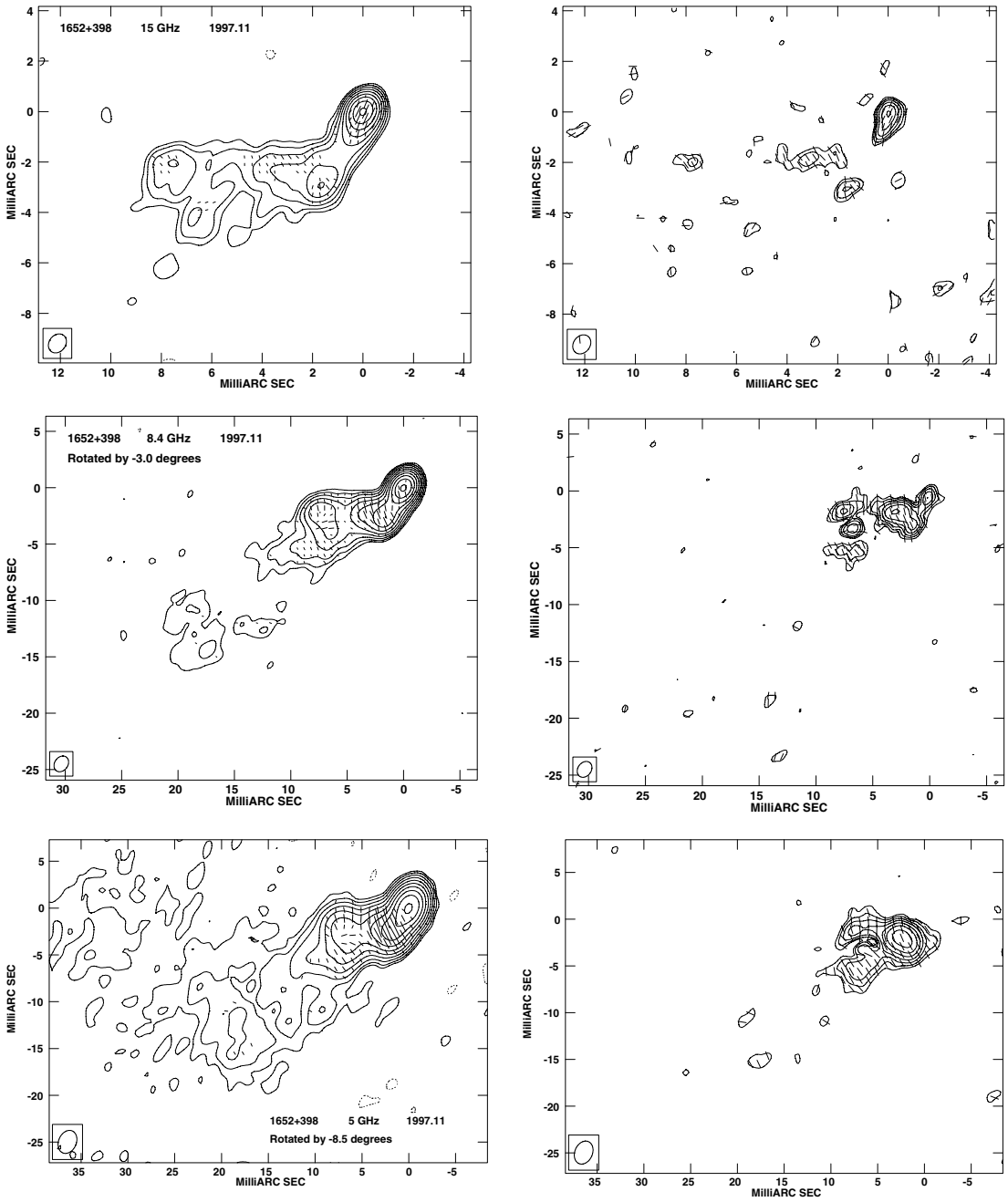

Figure 10. Left: *I* images of 1652+398 at epoch 1997.11 with contours increasing in steps of two and *P* vectors superimposed. Right: corresponding polarized flux images with contours increasing in steps of $\sqrt{2}$ and χ vectors superimposed. Top: 15 GHz, bottom *I* contours at ± 0.35 per cent of the peak brightness of 361 mJy beam^{-1}; bottom *p* contour at 17 per cent of the peak brightness of 10.3 mJy beam^{-1}. Middle: 8.4 GHz, bottom *I* contours at ± 0.175 per cent of the peak brightness of 440 mJy beam^{-1}; bottom *p* contour at 17 per cent of the peak brightness of 6.0 mJy beam^{-1}. Bottom: 5 GHz, bottom *I* contours at ± 0.175 per cent of the peak brightness of 519 mJy beam^{-1}; bottom *p* contour at 10 per cent of the peak brightness of 11.7 mJy beam^{-1}.

Attridge et al. (1999) initially interpreted the polarization structure they observed in $1055+018$ as being owing to a combination of transverse shocks giving rise to a dominant $\boldsymbol{B}$ field perpendicular to the jet near the jet axis, and interaction with the surrounding medium giving rise to a dominant longitudinal $\boldsymbol{B}$ field near the jet edges. In this picture, a shear layer forms because the plasma near the edges of the jet is slowed by its interaction with the ambient medium (Laing 1996), simultaneously enhancing the longitudinal component of the $\boldsymbol{B}$ field. The jet-edge polarization is strongest where the interaction between the jet and medium is strongest; the change in the location of the edge polarization in $1418+546$ from the northern to the southern edges of the jet from epoch to epoch could reflect changes in the strength of interaction on the two sides of the jet.

However, an alternative, and overall simpler, interpretation is that the transverse polarization structure observed in the jets of 1055+018 and the three BL Lac objects considered here indicates the presence of a helical or toroidal $\boldsymbol{B}$ field associated with the jet. Our tentative detection of interknot polarization in 1055+018 with

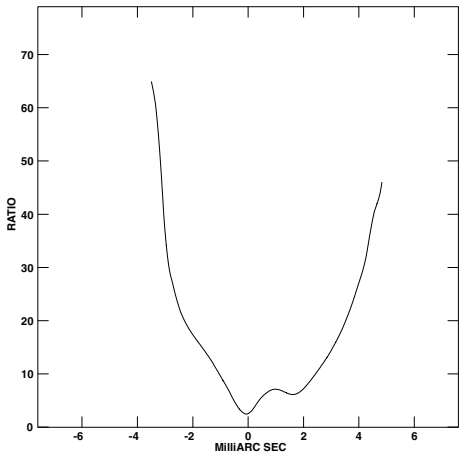

Figure 11. The degree of polarization profile across the jet of Mkn 501 at 5 GHz at 7.5 mas from the core along a position angle of 9°.

the ***E*** well aligned with the local jet direction supports this possibility. When such a helical ***B*** field is viewed at an angle differing from 90° to the jet axis in the source rest frame, the ***B*** field near the ridge line of the jet is orthogonal to the jet, while the dominant ***B*** field at the edges of the jet becomes longitudinal, forming spine+sheath ***B***-field structures of the sort observed in the four objects considered here. For certain combinations of pitch angle and viewing angle, the degree of polarization can be appreciably higher at the jet edges than at the jet ridge line, as is observed for 1652 + 398 (Lyutikov et al. 2004). In this case, the asymmetry of the orthogonal polarization observed at the edges of the jets is determined by the pitch angle of the ***B***-field helix and the viewing angle; 90° jumps in the polarization angle such as those observed in 1418+546 can be explained by small changes in the viewing angle for different regions in the jet (Lyutikov et al. 2004).

Thus, our observations have demonstrated that spine–sheath polarization structures are not uncommon among AGN jets, but their origin remains unclear. They may be owing to the joint action of shocks in the jets and interaction between the jet and surrounding medium, as originally proposed by Attridge et al. (1999), or they may be an observational manifestation of helical ***B*** fields associated with the jets. The recent detection of Faraday-rotation gradients transverse to the VLBI jets of several BL Lac objects, including 1652+398, has been interpreted by Gabuzda et al. (2004) as betraying the presence of helical or toroidal jet ***B*** fields – the RM gradient is the result of the systematic variation in the line-of-sight ***B*** across the jet. Determination of whether the observed spine–sheath polarization structures represent further evidence for helical jet ***B*** fields or testify to interaction with a surrounding medium will require further multiwavelength polarization VLBI observations and modelling of the observed transverse polarization structures.

ACKNOWLEDGMENTS

The work was partly supported by the Russian Foundation for Basic Research (project code No. 02-02-16305) and INTAS Grant No. 2001–0669. The National Radio Astronomy Observatory is operated by Associated Universities, Inc., under cooperative agreement with the NSF. We gratefully acknowledge the VSOP Project, which is led by the Japanese Institute of Space and Astronautical Science in cooperation with many organizations and radio telescopes around the world. This research has also made use of data from the University of Michigan Radio Astronomy Observatory, which has been supported by the University of Michigan and the National Science Foundation. Finally, we would like to thank the anonymous referee for certain useful comments.

REFERENCES

Aaron S. E., 1996, PhD thesis, Brandeis Univ., MA
Aaron S. E., 1999, in Takalo L. O., Sillanpää A., eds, ASP Conf. Ser. Vol. 159, BL Lac Phenomenon. Astron. Soc. Pacific, San Francisco, p. 427
Appenzeller I., Thiering I., Zickgraf F.-J. et al., 1998, MNRAS, 117, 319
Attridge J. M., Roberts D. H., Wardle J. F. C., 1999, ApJ, 518, L87
Falomo R., Scarpa R., Bersanelli M., 1994, ApJS, 93, 125
Gabuzda D. C., 1999, New Astron. Rev., 43, 691
Gabuzda D. C., 2003, in Takalo L. O., Valtaoja E., eds, ASP Conf. Ser., Vol. 299, High Energy Blazar Astronomy. Astron. Soc. Pacific, San Francisco, p. 99
Gabuzda D. C., Gómez J.-L., 2001, MNRAS, 320, 49P
Gabuzda D. C., Pushkarev A. B., 2001, in Laing R., Blundell K., eds, ASP Conf. Ser. Vol. 250, Particles and Fields in Radio Galaxies. Astron. Soc. Pacific, San Francisco, p. 180
Gabuzda D. C., Wardle J. F. C., Roberts D. H., 1989, ApJ, 338, 743
Gabuzda D. C., Pushkarev A. B., Cawthorne T. V., 1999, MNRAS, 307, 725
Gabuzda D. C., Pushkarev A. B., Cawthorne T. V., 2000, MNRAS, 319, 1109
Gabuzda D. C., Murray É., Cronin P., 2004, MNRAS, 351, 89
Giroletti M. et al., 2004, ApJ, 600, 127
Hughes P. A., Aller H. D., Aller M. F., 1989, ApJ, 341, 68
Impey C. D., Tapia S., 1990, ApJ, 354, 124
Kim K. T., Tribble P. C., Kronberg P. P., 1991, ApJ, 379, 80
Laing R., 1980, MNRAS, 193, 439
Laing R., 1996, Hardee P. E., Bridle A. H., Zensus J. A., eds, ASP Conf. Ser. Vol. 100, Energy Transport in Radio Galaxies and Quasars. Astron. Soc. Pacific, San Francisco, p. 241
Lister M. L., Marscher A. P., Gear W. K., 1998, ApJ, 504, 702
Lyutikov M., Pariev V. I., Gabuzda D. C., 2004, MNRAS, submitted
Markarian B. E., Lipovetskii V. A., 1974, Astrofizika, 10, 307M
Murphy D., Browne I., Perley R., 1993, MNRAS, 264, 298
Perley R. A., 1982, ApJ, 87, 859
Pushkarev A. B., 2001, Astron. Rep., 45, 667
Pushkarev A. B., Gabuzda D. C., 2000, in Conway J., Polatidis A., Booth R., eds, Proceedings of the 5th EVN Symposium, Onsala Space Observatory, Gothenburg, p. 63
Quinn J., Akerlof C. W., Biller S. et al., 1996, ApJL, 456, L83
Roberts D. H., Gabuzda D. C., Wardle J. F. C., 1987, AJ, 323, 536
Roberts D. H., Wardle J. F. C., Brown L. F., 1994, AJ, 427, 718
Rudnick L., Jones T. W., 1983, AJ, 88, 518
Rusk R., 1988, PhD Thesis, University of Toronto, Toronto, Canada
Stickel M., Fried J. W., Kühr H., 1989, A&AS, 80, 113
Stickel M., Fried J. W., Kühr H., 1993, A&AS, 98, 393
Wardle J. F. C., Cawthorne T. V., Roberts D. H., Brown, L. F., 1994, ApJ, 437, 122
Wilkes B. J., Wright A. E., Jauncey D. L., Peterson, B. A., 1983, PASAu, 5, 2W
Wurtz R., Stoke J. T., Yee H. K. C., 1996, ApJS, 103, 109

This paper has been typeset from a TEX/LATEX file prepared by the author.